Structural Engineering and Mechanics, Vol. 16, No. 4 (2003) 371-390
DOI: http://dx.doi.org/10.12989/sem.2003.16.4.371

Study on a seismic slit shear wall with cyclic experiment and macro-model analysis

Huanjun Jiang† and Xilin Lu‡

Research Institute of Structural Engineering and Disaster Reduction, Tongji University, 1239 Siping Road, Shanghai, P.R. China

A. K. H. Kwan‡ and Y. K. Cheung‡†

Department of Civil Engineering, The University of Hong Kong, Pokfulam Road, Hong Kong

(Received February 18, 2002, Accepted June 28, 2003)

Abstract. The concept of the seismic slit shear wall was proposed in the early 1990's. A series of experimental and theoretic studies on the wall with reinforced concrete short connecting beams cast in the slit were carried out. In this paper another type of slit shear wall is studied. It is one with vertical slit purposely cast within the wall, and the rubber belt penetrated by a part of web shear reinforcement as seismic energy-dissipation device is filled in the slit. Firstly, an experiment under cyclic loading was carried out on two shear wall models, one slit and the other solid. The failure mechanism and energy-dissipation capacity are compared between the two different models, which testifies the seismic performance of the slit wall improved significantly. Secondly, for engineering practice purpose, a macroscopic analytical model is developed to predict the nonlinear behavior of the slit shear wall under cyclic loading. The mechanical properties of each constituent elements of this model are based on the actual behavior of the materials. Furthermore, the effects of both the axial force and bending moment on the shear behavior are taken into account with the aid of the modified compression-field theory. The numerical results are verified to be in close agreement with the experimental measurements.

Key words: shear wall; macroscopic model; energy dissipation; hysteretic model; cyclic loading.

1. Introduction

Reinforced concrete shear wall structures constitute a large stock of tall buildings, especially in seismic regions. However, due to their high lateral stiffness, RC shear walls tend to attract large amount of seismic energy as well as seismic loads, causing severe damages that concentrate at the base and are generally very difficult to be repaired (Aristizabal-Ochoa 1987). Most of the current seismic design codes in the world provide the design principles for RC shear wall that the plastic hinge region is prescribed at the base of the wall where yielding is allowed and considerate reinforcement details are afforded. In this way, the main structural components are actually allowed sacrificed to dissipate input seismic energy. To prevent shear walls suffering severe damages

† Associate Professor
‡ Professor
‡† Honorary Professor

concentrating at the base and to improve their seismic energy-dissipation capacity, a slit shear wall was proposed (Kwan *et al.* 1993). It was one with purposely built-in vertical slit along the centroidal axis of the wall, and energy-dissipation devices are installed in the slit connecting the two pieces of narrower walls. In the earlier research, a series of experimental and theoretical studies on the slit wall with RC short connecting beams cast in the slit were carried out (Cheung *et al.* 1993, Kwan *et al.* 1994, and Lu *et al.* 1997). In this paper, another type of slit wall with rubber belts and steel bars installed in the slit as energy-dissipation devices is studied. In order to verify this concept, two RC shear wall models, one slit and the other solid, were tested under cyclic lateral loading. The detailed descriptions and analysis for this test will be introduced here.

Finite element method was developed for this shear wall system (Lu *et al.* 2000). However, for engineering practice purpose, the macroscopic model is more desirable, due to its capability of reasonably simulating the main characteristics of shear walls by one element for one story to simplify modeling and reduce computational efforts. Several different types of macroscopic models for shear walls have been developed, ranging from simple one-dimensional beam element to complicate three-dimensional wall panel model. The equivalent beam model (EBM) is applied popularly in practice, but in this model there is a fatal defect that the assumption is adopted that rotations always occur around the centroidal axis and the fluctuation of the cross-section neutral axis is disregarded even if the wall gets into inelastic state. Thus, such important features as rocking of the wall, outtriggering interaction with the structural components surrounding the wall can not be adequately reflected.

The multi-vertical-line-element model (MVLEM) remedying the defect of EBM was proposed (Valcano *et al.* 1988). In this model the shear wall was represented by a set of nonlinear vertical and horizontal springs connected by two rigid beams at the top and the bottom. By using this model, desirable agreement between predicted and measured nonlinear response was obtained (Fu *et al.* 1992 and Linde *et al.* 1994). However, the shear response of the horizontal spring was not adequately predicted, particularly when shear effects were significant. Moreover, the effects of both the axial force and the bending moment on the shear behavior of the wall were not taken into account. The flexural and shear displacement components were predicted independently. In fact the behavior of walls is strongly influenced by the interaction between axial force flexure and shear (Colotti 1993). In addition, for lack of experimental data, the axial force-deformation relationship of the vertical spring proposed in the literature was based on empirical assumptions. To improve the prediction of the nonlinear behavior of RC structural walls subjected to static or dynamic loads, a modified MVLEM is developed in this paper. The constitutive model for the vertical spring is based on the actual mechanical behavior of two constituent materials, concrete and steel. The modified compression-field theory (MCFT) is incorporated to predict the shear response of the horizontal spring, considering the effects of axial force and bending moment. Extensive research has been conducted to simulate the hysteretic behavior of RC members (Ozcebe *et al.* 1989, Stevens *et al.* 1991, and Wu *et al.* 1996). The hysteretic models, provided by previous research for different RC structural components, are used here to predict the hysteretic response of the two test wall models.

2. Description of the test

2.1 Test models

Two RC shear wall models, one slit vertically (named as DSW-T) and the other solid (named as

SSW-T), were constructed. They were both four-story 1/4-scale models with the aspect ratio of 2.8, identical in size as well as in reinforcement ratios. The overall dimensions and reinforcement details are shown in Figs. 1 and 2. Each model consisted of the wall itself with one boundary column at each edge, the top loading beam and the base beam for fixing the wall model onto the supporting block. In model DSW-T a piece of rubber belt with the same thickness as the wall was filled in the 10 mm wide slit. The top loading beam and all the horizontal steel bars were cut at the vertical slit except eight bars in each story penetrating the rubber belt and connecting the two piers of the wall, four at the mid-height of each story and the other four at each floor level respectively. Two pieces of smooth steel plate were embedded at both sides of the slit to let the two piers of the wall slide with less restraint as possible.

Normal weight concrete and mild steel bars were used for the construction of the models. The two models were cast vertically, story by story. The compressive strengths of the concrete as determined by testing cubes cast of the same batches of materials and cured alongside the models were 36.0 MPa and 37.2 MPa for SSW-T and DSW-T respectively. The round steel bars with the diameter of 6.5 mm were used as reinforcement throughout. The yield and ultimate strengths of the steel bars were 289 MPa and 465 MPa respectively. The ratios of vertical and horizontal reinforcement in each wall model were approximately 1.41% and 0.98%. All vertical bars in the models were properly anchored into the base beams.

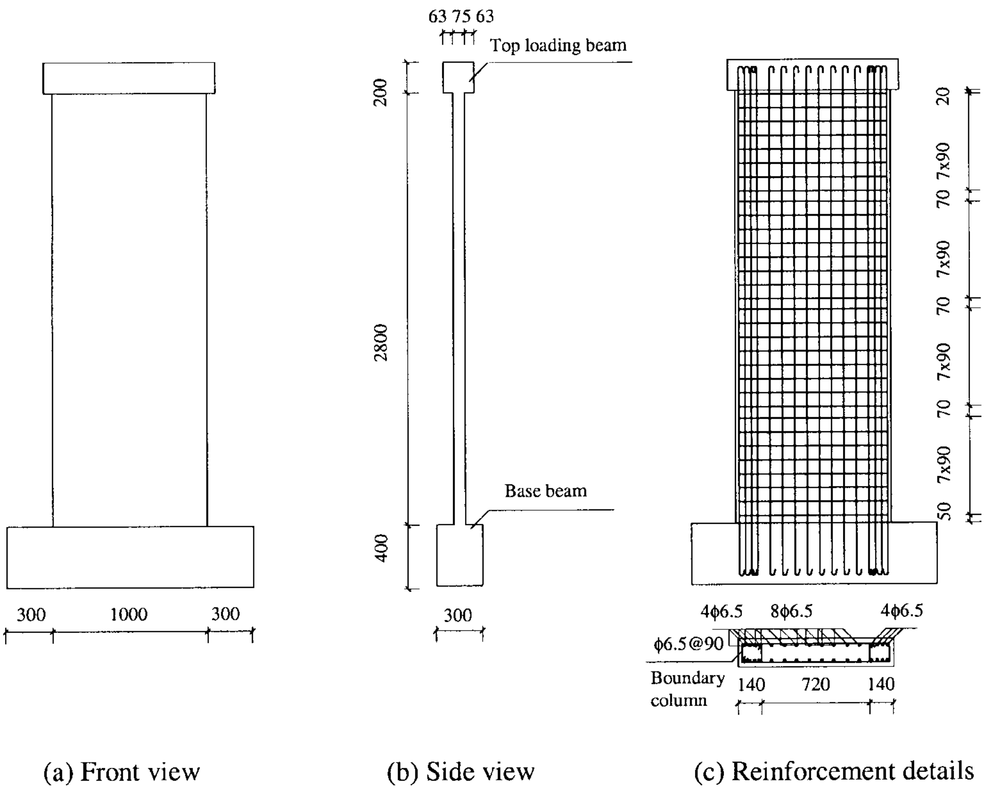

Fig. 1 Details of the solid shear wall model

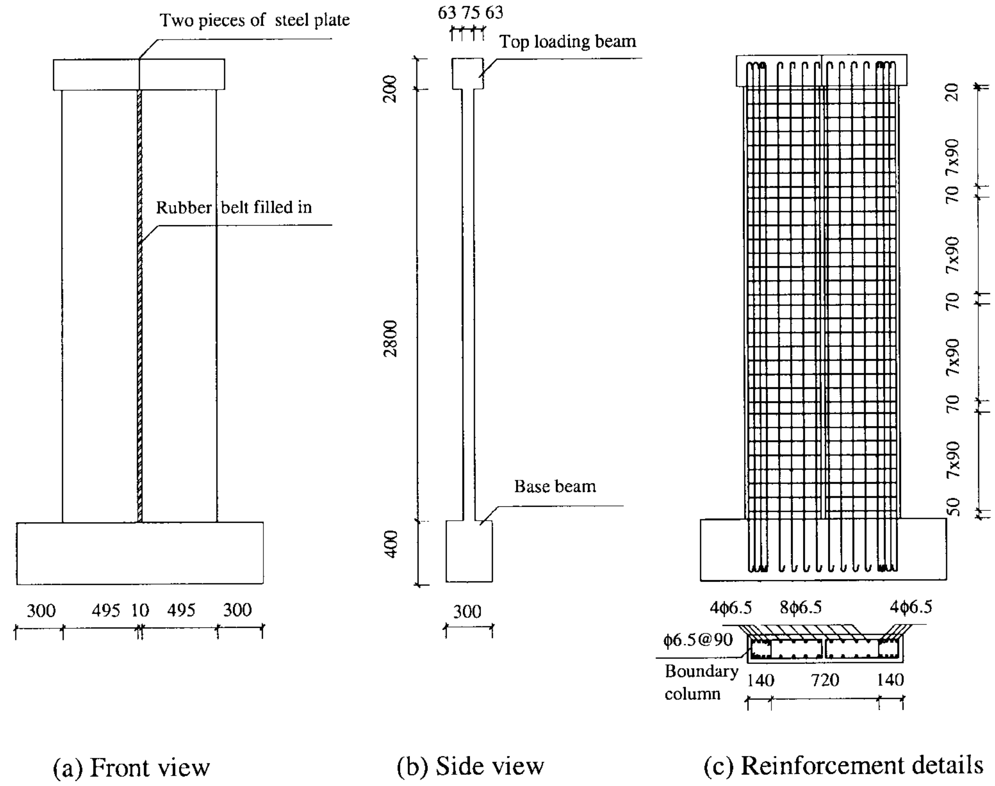

Fig. 2 Details of the slit shear wall model

2.2 Test set-up and program

The models were fixed on the supporting block as vertical cantilevers, as shown in Fig. 3. The vertical compressive load was applied on the top loading beam in advance of the application of the horizontal load by two hydraulic jacks reacting on a steel frame, which could be considered uniformly distributed through the loading beam to the wall models. The horizontal load was applied through double-acting hydraulic actuator on the upper one-third point of a rigid steel beam supported at the top and the mid-height levels of the models. In other words, the horizontal load provided by the hydraulic actuator was separated into two parts, two-thirds assigned to the top level and one-third to the mid-height level, consistent with the inverse triangle distribution. To prevent the models from losing out-plane stability, a steel brace with two rollers was set to support the two side faces of the models, which could constrain the out-plane movement of the models but let the models deform in plane without restraint. The external instrumentation consisted of a force sensor and a series of horizontal and vertical displacement sensors installed at different levels. Strain gauges were used to measure strains of the flexural bars and stirrups at specific locations.

During testing, the compressive load on the models was kept constant with the amount of 200 kN while the horizontal load was applied cyclically at two stages, with the amount varying. At the initial stage, the loading was force-controlled, with one cycle at each load amplitude. After the vertical steel bars in the boundary columns yielded, the loading became displacement-controlled,

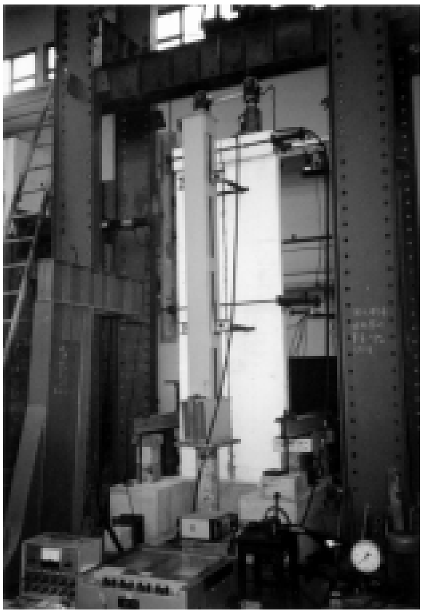

Fig. 3 Test set-up

with three cycles at each displacement amplitude, in order to assess the structural characteristics of the models beyond their strength limits. The displacement amplitudes (DA) of each cycle for SSW-T and DSW-T were incremented in steps of the multiple of the yield displacement (δ_y). Both of the models were loaded to failure defined as the state at which the loading capacity dropped to 85% of the ultimate load.

2.3 Failure process

2.3.1 Model SSW-T

Fig. 4(a) shows the crack pattern of this model. When the horizontal load reached about 50 kN, the first flexural crack, roughly horizontal, appeared at the bottom of the boundary columns. As the load increased, more new roughly horizontal cracks formed above the first crack in the first story. Then the former cracks extended to the web wall, and the previously formed cracks opened with larger width. As the applied load got to about 100 kN, tensile yielding occurred at the bottom of the vertical steel bars in the boundary columns, identified by the strain gauge readings. The cracks opened and closed alternatively as the loading direction was reversed. At that time, the strains in the stirrups were still comparatively small, with the maximum amount of 243 micro-strain. Hereafter, the loading became displacement-controlled. During the three cycles with DA equal to $2\delta_y$, flexural cracks formed drastically in the first story, similar cracks began to appear in the two edges of the second story. The flexural cracks in the upper part of the boundary columns extended to the web wall and showed a downward trend. At the bottom the vertical steel bars in the web close to the boundary columns yielded. The horizontal cracks at the bottom level joined up. When DA reached $3\delta_y$, the vertical bars at the bottom of the centroidal axis also yielded. During the cycles with DA equal to $4\delta_y$, at the bottom of the boundary columns the vertical bars buckled, the concrete crushed and spalled. During the cycles with DA equal to $6\delta_y$, the crushing zone extended to the inner web wall gradually, and all of the vertical steel bars at the bottom experienced yielding while all of the stirrups were far from yielding. At the end of these cycles, the applied load dropped to less than 85% of the ultimate load, the test stopped accordingly. The final failure pattern of this model is shown in Fig. 5(a).

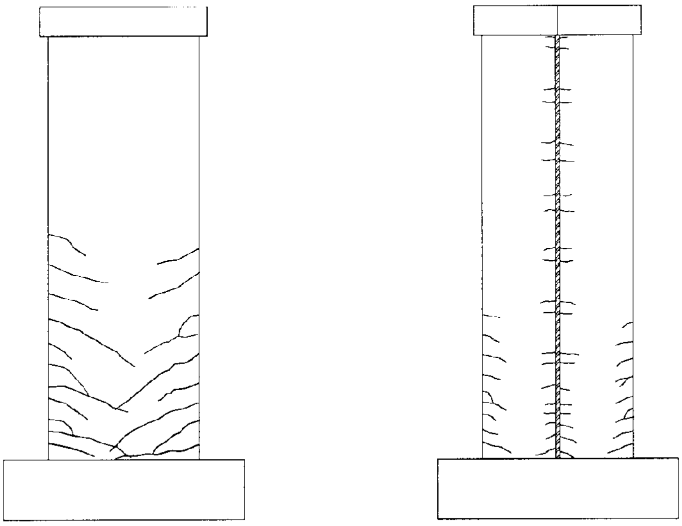

(a) SSW-T (b) DSW-T

Fig. 4 Crack pattern

(a) SSW-T (b) DSW-T

Fig. 5 Failure modes

2.3.2 Model DSW-T

Fig. 4(b) shows the crack pattern of this model. When the applied load reached about 45 kN, the first flexural crack formed at the bottom of the boundary columns. As the load increased, obvious relative sliding between the rubber belt and the two wall piers was observed. When the applied load varied from 50 kN to 60 kN, horizontal split cracks appeared adjacent to the slit at the levels where the horizontal steel bars penetrated the rubber belt from the first to the fourth story successively. Shortly afterwards, the flexural cracks also appeared at the bottom of the web wall close to the slit. During the period when the load varied from 65 kN to 75 kN, the relative sliding deformations between the rubber belt and the wall piers got larger and larger, and there were some sand particles falling down from the interfaces. At the same time, the horizontal bars penetrating the rubber belt yielded from the first to the fourth story successively. When the load reached about 80 kN, the vertical bars at the bottom of the boundary columns yielded. The loading became displacement-controlled hereafter. During the cycles with DA equal to $2\delta_y$, the former flexural cracks in the boundary columns extended to the web wall, and some new flexural cracks appeared in the two edges of the second story. The vertical bars at the bottom close to the slit also yielded. As the applied displacement increased, the concrete covers of the horizontal bars penetrating the rubber belt at both sides of the slit spalled from the first to the fourth story successively. During the cycles with DA equal to $4\delta_y$, at the bottom of the boundary columns the vertical bars buckled, the concrete crushed and spalled. As the applied displacement increased further, more concrete covers of the horizontal bars close to the slit spalled, and larger sliding deformation between the rubber belt and the wall piers took place. The flexural cracks were observed even in the edges of the third story. During the cycles with DA equal to $7\delta_y$, the horizontal cracks at the bottom of the wall joined up, and the crushing zone at the bottom level extended to the web wall gradually. When the applied displacement reached about $9\delta_y$, the test stopped since the loading capacity dropped to less than 85% of the ultimate load. The final failure pattern of this model is show in Fig. 5(b).

2.4 Comparison between the two models

2.4.1 Failure mechanism

In both models the first formed cracks were similar, due to bending tensile. Then different failure process took place. SSW-T behaved like a cantilever beam, and it finally failed by buckling of the longitudinal bars and crushing of the concrete in the compressive zone. The damages concentrated at the base of the model. In the case of DSW-T the sliding deformation between the rubber belt and the wall piers occurred. Then the damages appeared along the slit, which made the connection between the two wall piers weakened. After the energy-dissipation devices experienced more damages, the independence of the two wall piers became more obvious. In the end, each wall pier followed the same failure pattern as SSW-T. The damages at the base of DSW-T were lightened much more than those of SSW-T. Furthermore, the slit wall may be regarded as an innovative application of the "hierarchic plastification sequence" design philosophy proposed by Paulay (1983). The energy-dissipation devices tend to yield and be damaged firstly when the structure is subjected to seismic attack, which brings about an additional line of defense for the main structure.

2.4.2 Energy-dissipation mechanism

The energy-dissipation capacity of the structures, as one of the most important characteristics reflecting the seismic performance, depends mainly on the energy-dissipation mechanism. In the case of SSW-T it dissipated energy only by suffering damages on itself, such as cracking and crushing of the concrete, yielding and buckling of the steel bars and so on, and hence the energy-dissipation capacity was very limited. As DSW-T was concerned, the energy was dissipated mainly by the deformation of the rubber belt, the friction sliding in the interfaces between the rubber belt and the wall piers, and the cyclic yielding of the horizontal bars crossing the slit, so the energy-dissipation capacity was enhanced significantly. By calculating the enclosed areas of the base shear versus top displacement hysteretic curves, the energy dissipated in the test models was obtained. The dissipated energy in the test was 71.7 kN · m and 102.6 kN · m for SSW-T and DSW-T respectively.

2.4.3 Hysteretic curves of base shear versus top displacement

The hysteretic curves of base shear versus top displacement for the two models are shown in Fig. 6. The common characteristics of the curves are as follows: the hysteretic hoops remained stable, with small irrecoverable deformation and enclosed areas, until the yielding of the main longitudinal bars happened. During the three cycles with the same DA, the strength and reloading stiffness degraded obviously between the first and the second cycle while the unloading stiffness degraded hardly, and the degradation of these values tended to slow down evidently in the third cycle. The envelopes of the overall force-displacement relation can be easily obtained from Fig. 6. Both of the two models showed good ductility although DSW-T exhibited more ductile behavior, with a gentler post-ultimate descending segment in the envelope. The ductility ratio of top displacement of DSW-T was 35% larger than that of SSW-T.

Table 1 summarizes the main characteristics of the models at different states. All the values are the averages of the two loading directions. The elastic lateral stiffness and the ultimate load of DSW-T were both 72% of those of SSW-T, which implies that slit walls resemble coupled shear walls and the behavior of slit walls may be inferred to some extent from that of coupled shear walls accordingly.

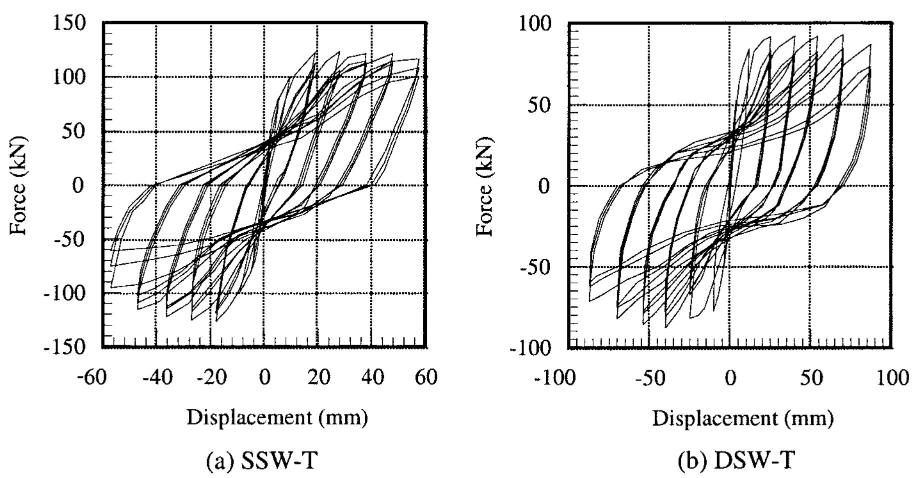

Fig. 6 Base shear versus top displacement hysteretic curves

Table 1 Main characteristics of test models

Model number	Cracking load (kN)	Cracking displ. (mm)	Elastic stiffness (kN/mm)	Yielding load (kN)	Yielding displ. (mm)	Ultimate load (kN)	Ultimate displ. (mm)	Ductility ratio
SSW-T	52.12	2.17	24.04	99.48	9.21	124.65	57.06	6.2
DSW-T	44.27	2.56	17.29	79.33	10.38	90.04	87.20	8.4

3. Analytical model

3.1 Description of analytical model

Fig. 7 shows the analytical model. The energy-dissipation device in the slit is represented by a nonlinear spring according to the previous shear-friction test carried out on this device (Lu *et al.* 1998), and the shear wall is represented by the macro wall element model MVLEM. In MVLEM the infinitely rigid beams at the top and the bottom are connected by some vertical truss elements paralleled to each other. The two outside truss elements represent the axial and flexural stiffness of the two boundary columns, and the other internal truss elements represent those of the central wall panel. The horizontal spring simulates the shear response of the wall member. Two rigid elements with the spacing of rh and $(1-r)h$ are placed between the horizontal spring and the bottom rigid beam, and between the horizontal spring and the top rigid beam respectively, in order to simulate the deformation of the wall under the expected curvature distribution along the height. The relative rotation between the top and bottom levels is assumed to be around the point ‘A’ located on the centroidal axis of the wall element. A suitable value for r can be determined on the basis of the expected curvature distribution along the height of the element. To account for the fact that there are hardly any points of contraflexure and the bending moment varies slowly in the inter-story height, the assumption of uniform curvature distribution is suitable, and the value of r equal to 0.5 is derived accordingly.

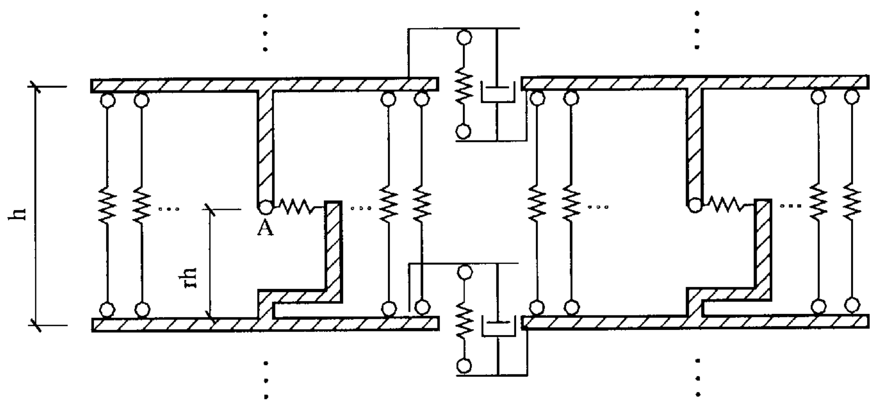

Fig. 7 Analytical model

3.2 Constitutive model for axial truss element

Since few tests on RC axial truss element under cyclic loading have been carried out so far, the hysteretic models for the axial force-deformation relationship were proposed on the basis of many empirical assumptions in the literature, which could be classified as two types, one considered the contributions afforded by concrete and steel integrally as one spring and the other independently as two springs in parallel, concrete spring and steel spring. The former one was short of reliable foundation, and the latter one neglected concrete-steel interaction, one of the most important features in RC structural members. In this research the modification of the latter one is developed by using average stress versus average strain relationship based on many tests to take concrete-steel interaction into account. The average strain of concrete is equal to that of steel, which is measured along a length that crosses several cracks including not only the strain of the concrete itself but also the strain contributed by the crack widths. Combining the contributions provided by steel and concrete, the axial force-deformation relationship can be obtained.

3.2.1 The stress-strain hysteretic model for concrete

The stress-strain hysteretic model for concrete is shown in Fig. 8, where the tensile stiffening representing the stiffening of the steel bars and cracking surface effect are appropriately considered (Wu *et al.* 1996). For the concrete in the boundary columns, the stress-strain curves for confined concrete proposed by Scott *et al.* (1982) are adopted here, and the hysteretic rules are assumed as same as those for the unconfined concrete.

3.2.2 The stress-strain hysteretic model for reinforcement

The average stress-strain relationship of mild steel bars embedded in concrete is used, considering the stiffening effect due to concrete. The bilinear average stress-strain curves developed by Hsu (1993) are adopted as the envelope curves, and the equations of these two lines are given as follows:

$$\sigma_s = E_s \varepsilon_s \qquad \sigma_s \le f_y' \tag{1}$$

$$\sigma_s = (0.91 - 2B) f_y + (0.02 + 0.25B) E_s \varepsilon_s \qquad \sigma_s > f_y' \tag{2}$$

where

$$f_y' = (0.93 - 2B) f_y \tag{3}$$

$$B = \frac{1}{\rho}\left(\frac{f_{cr}}{f_y}\right)^{1.5} \tag{4}$$

where E_s is the modulus of elasticity of reinforcement, ρ is the reinforcement ratio, f_y is the yield strength of reinforcement, and f_{cr} is the cracking strength of concrete. The hysteretic model is shown in Fig. 9. From the work of Santhanam (1979) the stiffness degradation factor γ is taken as 0.5.

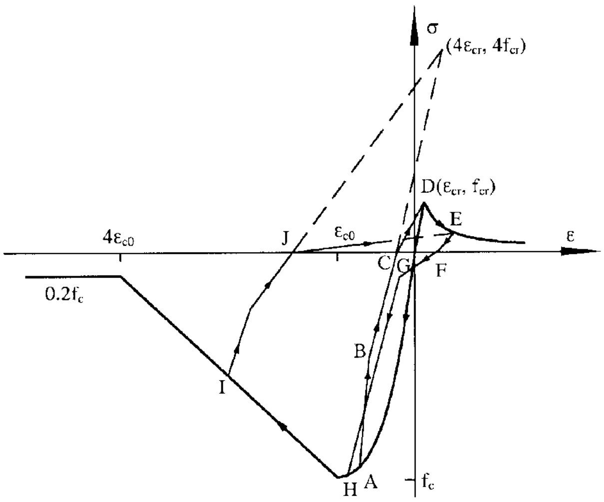

Fig. 8 Stress-strain hysteretic model for concrete

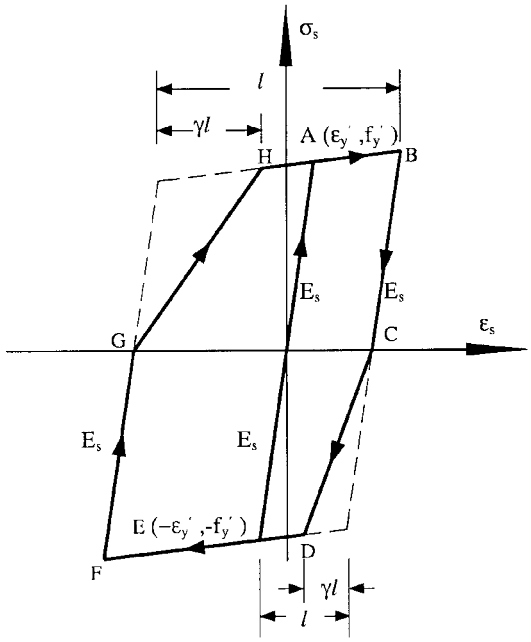

Fig. 9 Stress-strain hysteretic model for reinforcement.

3.3 Constitutive model for shear spring

3.3.1 Calculation of shear force-shear deformation envelope

In most of the previous research on the macro element models developed for shear walls, the effects of axial force and bending moment on the shear behavior were neglected, and the shear and flexural deformation components of the wall were calculated independently. Nevertheless, the interaction between axial force flexure and shear does exist, especially after the wall reaches yielding (Saatcioglu *et al.* 1980). To make up this deficiency, the modified compression-field theory is used to predict the shear response of the wall here. The wall panel is represented by a RC membrane element containing an orthogonal grid of reinforcement parallel to the edges, subjected to membrane stresses. The loads applied on the edges are roughly assumed uniformly distributed, described by average normal stress and shear stress as shown in Fig. 10. In this figure, the x- and y-directions represent the transverse and longitudinal directions respectively. The contribution of the reinforcement to the resistance of the element is expressed as $\rho_x\sigma_{sx}$ and $\rho_y\sigma_{sy}$ in the x- and y-directions respectively, where ρ is reinforcement ratio and σ axial stress in the reinforcement. The dowel action of reinforcement is neglected. The contribution of the concrete is expressed in terms of the average principal stresses σ_1 and σ_2 obtained by stress transformation from Mohr's circle of stresses. Combing the contributions provided by reinforcement and concrete, the equilibrium conditions can be expressed as:

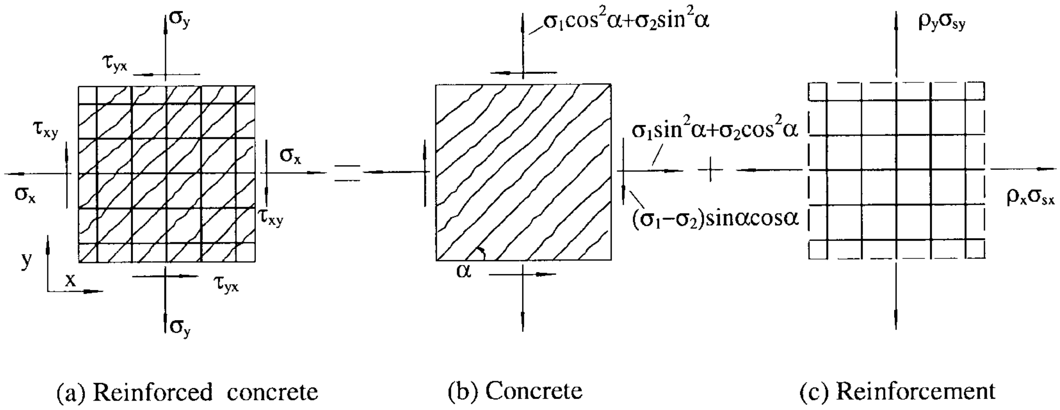

Fig. 10 Stress condition in membrane element

$$\sigma_x = \sigma_1 \sin^2\alpha + \sigma_2 \cos^2\alpha + \rho_x \sigma_{sx} \tag{5}$$

$$\sigma_y = \sigma_1 \cos^2\alpha + \sigma_2 \sin^2\alpha + \rho_y \sigma_{sy} \tag{6}$$

$$\tau_{xy} = (\sigma_1 - \sigma_2)\sin\alpha\cos\alpha \tag{7}$$

where α is the inclination angle of the compressive principle stress of concrete.

From Mohr's circle of strains the following equations can be obtained:

$$\varepsilon_1 = \frac{\varepsilon_x + \varepsilon_y}{2} + \sqrt{\left(\frac{\varepsilon_x - \varepsilon_y}{2}\right)^2 + \left(\frac{\gamma_{xy}}{2}\right)^2} \tag{8}$$

$$\varepsilon_2 = \frac{\varepsilon_x + \varepsilon_y}{2} - \sqrt{\left(\frac{\varepsilon_x - \varepsilon_y}{2}\right)^2 + \left(\frac{\gamma_{xy}}{2}\right)^2} \tag{9}$$

$$\tan(2\alpha) = \frac{\gamma_{xy}}{(\varepsilon_y - \varepsilon_x)} \tag{10}$$

The relationship between average principal stresses and average principal strains of concrete, derived by Vecchio *et al.* (1986) on the basis of test results, is adopted here. The formulas for compression are as follows:

$$\sigma_2 = \beta f_c' \left[2\frac{\varepsilon_2}{\varepsilon_0} - \left(\frac{\varepsilon_2}{\varepsilon_0}\right)^2\right] \tag{11}$$

where f_c' and ε_0 are the cylindrical compressive strength and the corresponding strain of concrete respectively,

$$\beta = \frac{1}{\left(0.8 - 0.34\frac{\varepsilon_1}{\varepsilon_0}\right)} \le 1 \tag{12}$$

These two formulas reflect the effect of strain softening in cracked concrete on compression under plane stress conditions. The formulas for tension are as follows:

$$\sigma_1 = E_c \varepsilon_1 \qquad 0 \le \varepsilon_1 \le \varepsilon_{cr} \tag{13}$$

$$\sigma_1 = \frac{f_{cr}}{(1 + \sqrt{200\varepsilon_1})} \qquad \varepsilon_1 > \varepsilon_{cr} \tag{14}$$

where E_c is the elastic modulus of concrete, f_{cr} and ε_{cr} are the cracking strength and the corresponding strain of concrete respectively. Eq. (14) describes the tension-stiffening effect after cracking. The constitutive curves of concrete under plane stress conditions are shown in Fig. 11. For steel the bilinear envelope shown in Fig. 9 is adopted. According to Hsu's work (1993), the post-yield stress in the steel embedded in concrete was also a function of the steel orientation, so modification should be made to Eqs. (2)-(3) as follows:

$$\sigma_s = \left(1 - \frac{2 - \alpha/45^{\circ}}{1000\rho}\right)[(0.91 - 2B)f_y + (0.02 + 0.25B)E_s\varepsilon_s] \tag{2a}$$

$$f_y' = \left(1 - \frac{2 - \alpha/45^{\circ}}{1000\rho}\right)(0.93 - 2B)f_y \tag{3a}$$

where the meanings of all the signs are as same as forementioned.

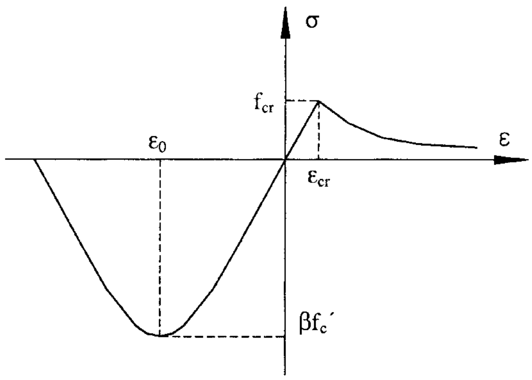

Fig. 11 Equivalent uniaxial stress-strain curves under plane stress conditions

To obtain the relationship between τ_{xy} and γ_{xy}, an iterative procedure is developed. Generally the stress components σ_x and σ_y are known in a given RC wall element, and then the following iteration procedure can be adopted:

(1) Select a value for γ_{xy}.
(2) Assume values for ε_x and ε_y.
(3) Calculate ε_1, ε_2, and α from Eqs. (8)-(10).
(4) Calculate σ_1 and σ_2 from Eqs. (11)-(14).
(5) Calculate σ_{sx} and σ_{sy} according to the relationship between the stress and the strain of steel, i.e., Eq. (1), Eq. (2a), Eq. (3a), and Eq. (4).

(6) Check the equilibrium Eq. (5) and Eq. (6). If they are satisfied within the acceptable tolerance, proceed to step 7; otherwise, go to step 2.
(7) Calculate τ_{xy} from Eq. (7).
(8) Increase γ_{xy} and repeat step (2)-(8).

The shear strain and shear stress are assumed to be constant over the height and the cross section of the wall element respectively, and then the relationship between shear force and shear deformation is obtained easily.

3.3.2 Hysteretic model

Fig. 12 shows the hysteretic shear model for RC members proposed by Ozcebe *et al.* (1989), which is adopted here. The developed rules for unloading and reloading branches of this model were obtained from a large number of test data. The comparisons between the experimental data obtained by different investigators and the predicted results produced by this model showed a good agreement. This model consists of an envelope, unloading and reloading branches under cyclic loading. The envelope is considered as same as the force-displacement relationship under monotonic loading, with well-defined cracking and yielding points. In this paper, it is obtained by the above-mentioned procedure. The cracking point is defined as the one at which the principal tensile stress is equal to cracking strength, and the yielding point is defined as the one at which the main flexural reinforcement yields.

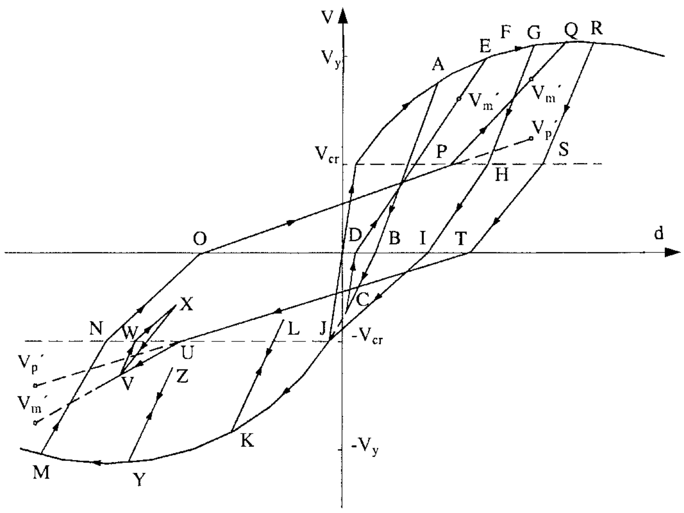

Fig. 12 Shear force-shear deformation hysteretic model

3.4 Constitutive model for energy-dissipation device in the slit

The characteristic points in the envelope are obtained on the basis of the theory for piles embedded in cohesive soil and the shear-friction mechanism. The detailed method can be read elsewhere (Lu *et al.* 1998). To be convenient for analysis, the envelope is simplified in tri-linear form. Based on the experimental data, the hysteretic model is established by regressing process, as shown in Fig. 13. The main hysteretic rules are as follows:

(1) Unloading follows the envelope until cracking load is exceeded. Beyond the cracking load unloading follows a straight line up to the zero load axis. When the yield load has not been exceeded, the slope of this line is determined by the following equation:

$$K_d = K_{de}\left(1 - 0.4 \times \frac{\Delta - \Delta_{cr}}{\Delta_y - \Delta_{cr}}\right) \tag{15}$$

where Δ is the displacement at which unloading starts, Δ_{cr} the displacement at cracking, Δ_y the displacement at yielding, and k_{de} the elastic stiffness of the energy-dissipation device. After the yield load is exceeded, the unloading stiffness is given by the following equation:

$$K_d = 0.6 \times K_{de}\left(\frac{\Delta}{\Delta_y}\right)^{-\frac{2}{3}} \tag{16}$$

(2) Initial loading and reloading follows the envelope until the cracking load is exceeded. If the cracking load is exceeded but the yielding load is not, reloading aims at the point where unloading starts. After the yielding load is exceeded, the reloading segment is divided into two straight lines the ordinate of whose intersection is the cracking load. Below the cracking load, the reloading stiffness is given by Eq. (17), and above it, is given by Eq. (18):

$$K_d = 0.14K_{de}\left(\frac{\Delta_m}{\Delta_y}\right)^{-1} \tag{17}$$

$$K_d = 0.20K_{de}\left(\frac{\Delta_m}{\Delta_y}\right)^{-0.5} \tag{18}$$

where Δ_m is the maximum displacement.

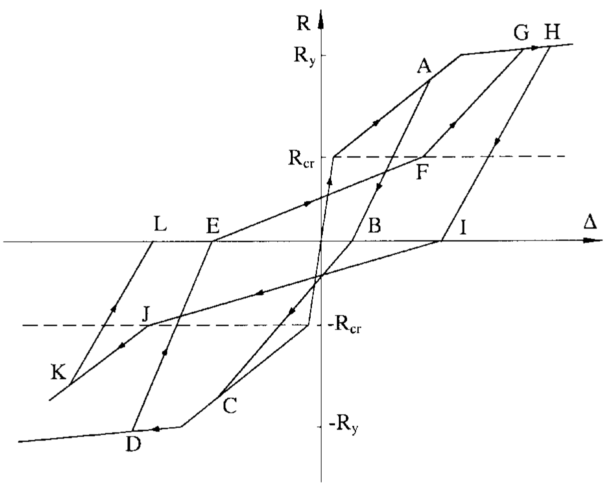

Fig. 13 Hysteretic model for energy-dissipation device

4. Numerical analysis of test

The analytical model mentioned in Sec. 3.1 is used to simulate the response of the two test models. In the calculation of the shear force-shear deformation envelope the longitudinal strain of the membrane element (ε_y) is approximately assumed to equal that of the vertical truss element located on the centroidal axis of the wall element, and the transverse stress (σ_x) is taken as zero. In order to obtain the descending segment of the skeleton curve, the displacement-controlled loading method is adopted. Fig. 14 shows the numerical models. The solid wall model is discretized in five wall elements, two elements for the first story and three elements for the upper three stories, and

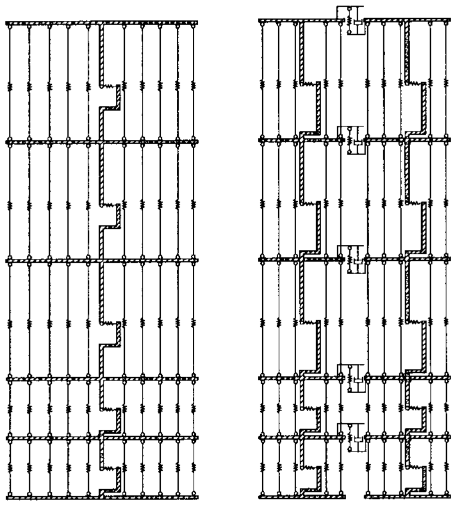

(a) SSW-T (b) DSW-T

Fig. 14 Numerical models

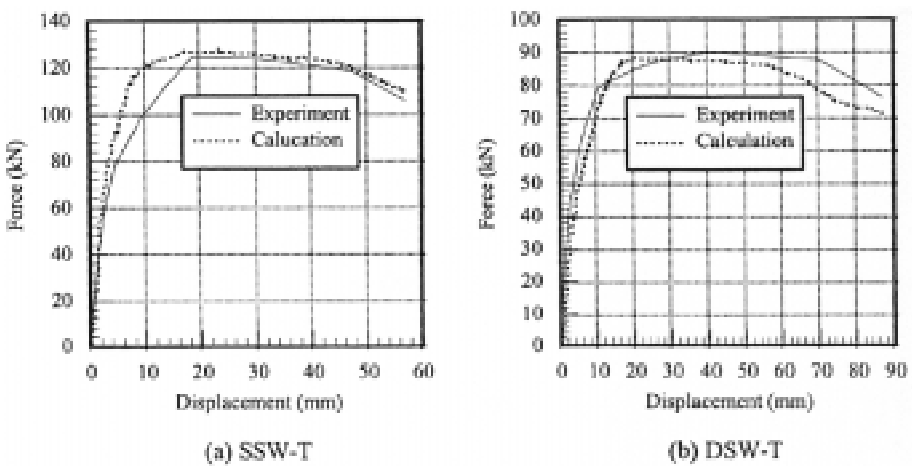

Fig. 15 Comparison between the experimental and calculated skeleton curves

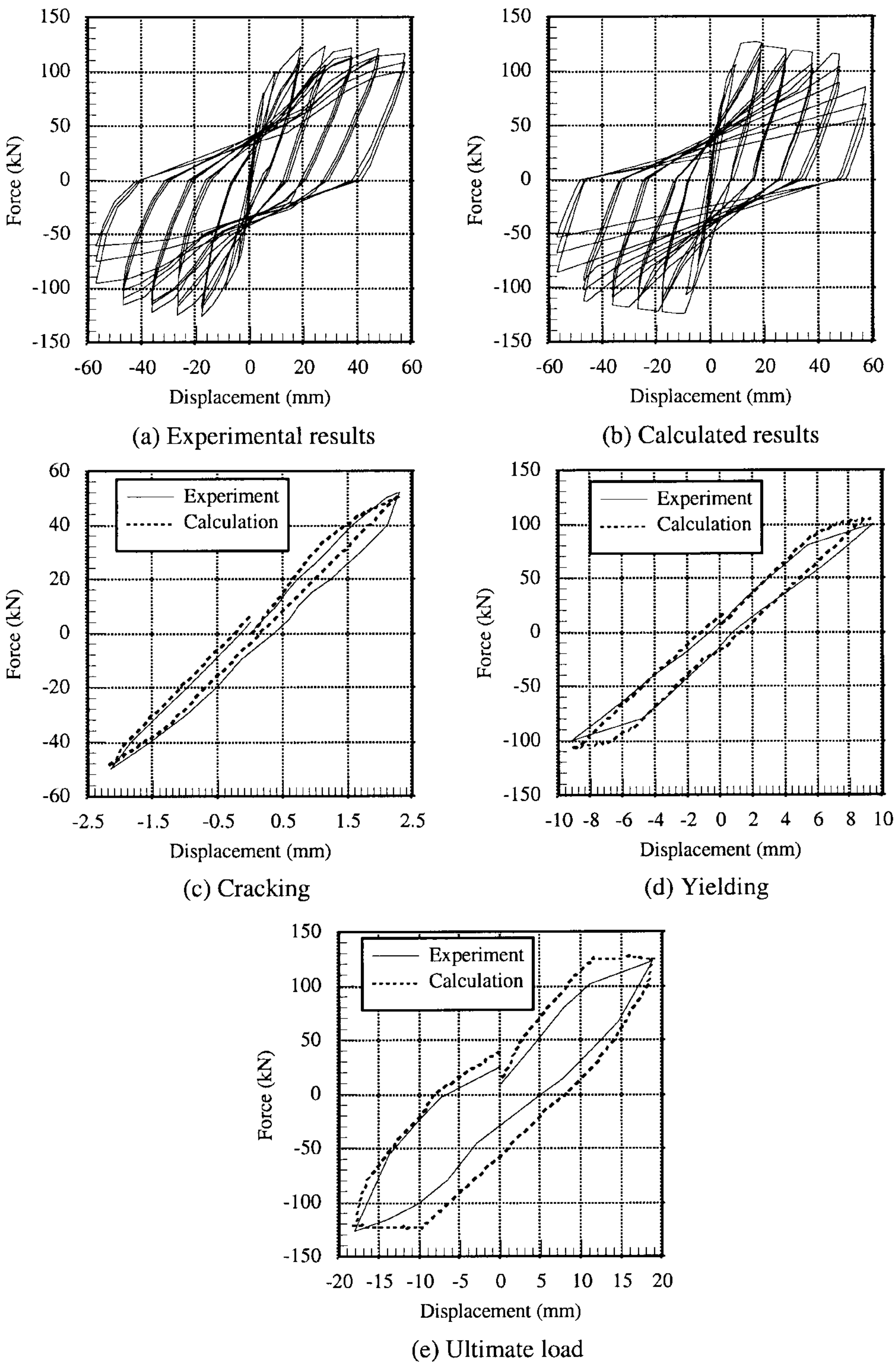

Fig. 16 Comparison between the experimental and calculated hysteretic curves for SSW-T

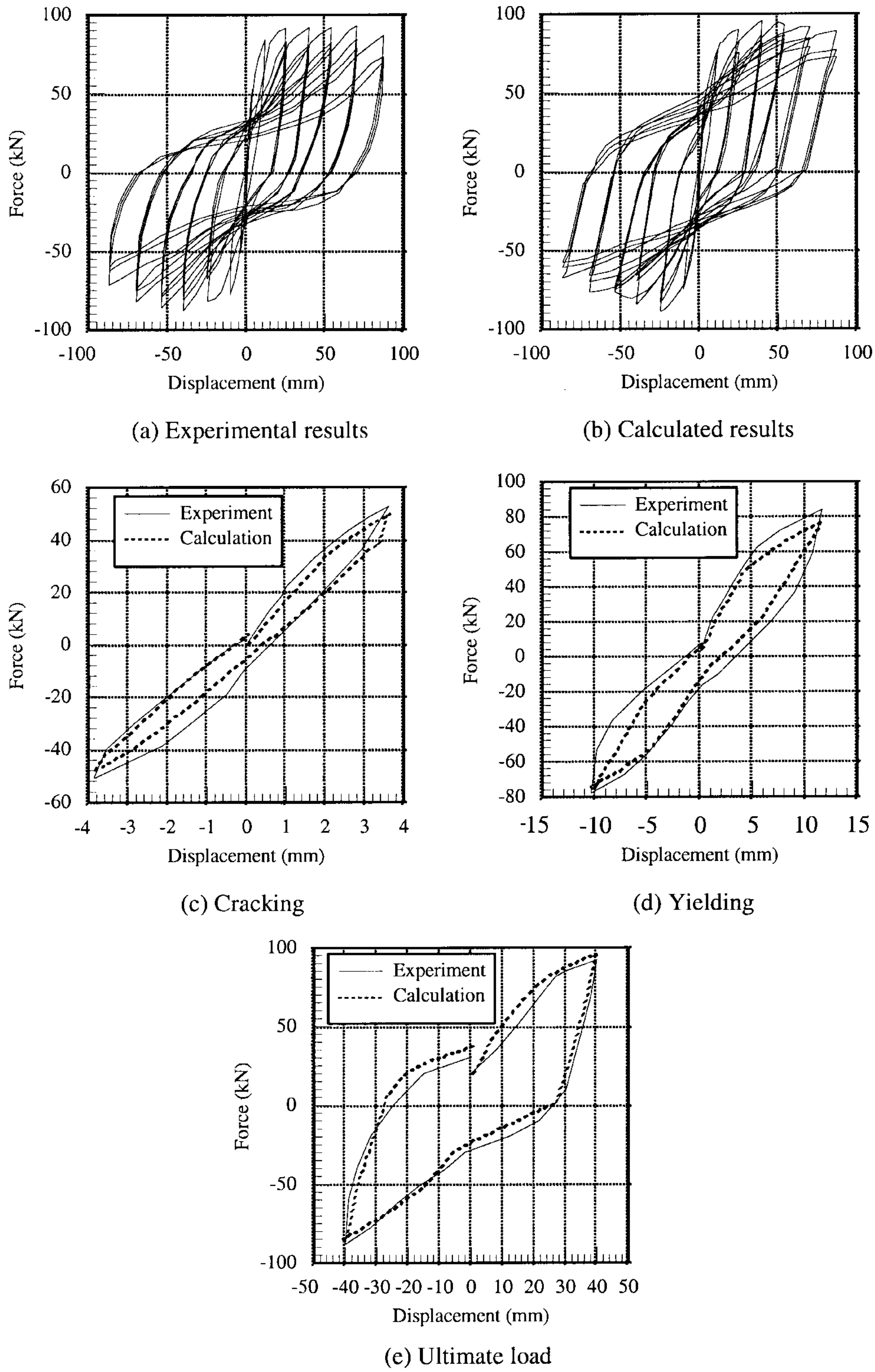

Fig. 17 Comparison between the experimental and calculated hysteretic curves for DSW-T

each wall element consists of ten vertical truss elements and one shear spring. The slit wall model is discretized in ten wall elements, four elements for the first story and six elements for the upper three stories, and each wall element consists of five vertical truss elements and one shear spring.

Firstly the base shear versus top displacement skeleton curves are calculated for the models under monotonic loading. The relationships between shear force and shear deformation for all the wall elements are stored in data files. Then the base shear versus top displacement hysteretic curves are calculated for the models under cyclic loading. In Figs. 15 to 17 the experimental and analytical results are compared, which show satisfactory agreement. To be convenient for comparison, the hysteretic loops at three different states are drawn individually.

According to the analytical results, the flexural deformation component is dominant in the total deformation in both of the two models. The ratios of the shear deformation to the total deformation are 6.0% and 3.6% in SSW-T and DSW-T respectively when the models behave elastically, but after the yield load is exceeded, these ratios add up to 11.2% and 7.4% respectively, and the shear deformation concentrates at the bottom wall element, being 86% and 91% of the total shear deformation in these two models. In the bottom wall element, the flexural yielding triggers the shear yielding. This phenomenon was also observed by Saatcioglu *et al.* (1980).

5. Conclusions

A seismic slit shear wall is studied in this paper. On the basis of above experimental study and theoretical analysis, the following conclusions can be drawn:

(1) The failure mode and the energy-dissipation mechanism are different between the proposed slit wall and the solid wall. The damages occurring at the joints of the slit have less effect on the overall structural safety and are easier to be repaired than the damages concentrating at the base in ordinary solid wall. According to the test results, it is feasible, simple and efficient to cast a vertical slit in shear wall and install energy-dissipation devices in it. Other energy-dissipation devices such as metallic dampers and friction dampers could try to be installed in the slit in future research. Since in shear wall systems the sliding deformation between the shear wall and the rubber belt is not large, the effect could be better if this slit shear wall is applied as infilled wall installed in frame structures.

(2) The modified MVLEM is developed to predict the nonlinear response of the two test shear wall models under cyclic loading. The mechanical properties of each constituent element in the wall model are based on the actual behavior of the materials rather than empirical assumptions. The axial force-deformation relationship of the vertical spring is based on the material constitutive laws of concrete and steel. The shear force-shear deformation envelope of the shear spring is obtained by using the modified compression-field theory. The effects of axial force and bending moment on the shear behavior of the shear wall are taken into account.

(3) The numerical results, obtained by using this macroscopic analytical model, are in good agreement with those of the test. This model with suitable constitutive laws, both capable of reproducing the nonlinear response of the slit shear wall with reasonable accuracy and simple enough to reduce computational efforts, is suitable for engineering practice.

References

Aristizabal-Ochoa, J.D. (1987), "Seismic behavior of slender coupled wall systems", *J. Struct. Eng.*, **113**(10), 2221-2234.

Cheung, Y.K., Kwan, A.K.H. and Lu, X.L. (1993), "Shear tests on simulated connecting beams in R.C. slit shear walls", *Proc. of the Institution of Civil Engineerings, Structures and Buildings*, **99**, 481-488.

Colotti, V. (1993), "Shear behavior of RC structural walls", *J. Struct. Eng.*, **119**(3), 728-746.

Fu, J., Shibata, A., Shibuya J.I. and Saito, T. (1992), "3-D inelastic earthquake response of RC frames with shear walls", *Proc. of the 10th World Conf. on Earthquake Engineering*, **8**, 4303-4308.

Hsu, Thomas T.C. (1993), *Unified Theory of Reinforced Concrete*. CRC Press, Inc., Florida, USA.

Kwan, A.K.H., Cheung, Y.K. and Lu, X.L. (1994), "Large scale model tests of reinforced concrete slit shear walls", *Int. J. Structures*, **14**(2), 63-82.

Kwan, A.K.H., Lu, X.L. and Cheung, Y.K. (1993), "Elastic analysis of slit shear walls", *Int. J. Structures*, **13**(2), 75-92.

Linde, P. and Bachmann, H. (1994), "Dynamic modeling and design of earthquake-resistance walls", *Earthq. Eng. Struct. Dyn.*, **23**(12), 1331-1350.

Lu, X.L. and Jiang, H.J. (1998), "Resistance analysis of shear-transfer interface of shear walls dissipating energy along vertical direction", *Academic Periodical Abstracts of China*, **4**(2), 241-244.

Lu, X.L., Wu, X.H. and Meng, L. (1997), "Seismic behavior of a new type of seismic energy dissipation shear wall system", *Struct. Eng. Mech. An Int. J.*, **5**(2), 167-175.

Lu, X.L. and Wu, X.H. (2000), "Study on a new shear wall system with shaking table test and finite element analysis", *Earthq. Eng. Struct. Dyn.*, **29**(10), 1425-1440.

Ozcebe, G. and Saatcioglu, M. (1989), "Hysteretic shear model for reinforced concrete members", *J. Struct. Eng.*, **115**(1), 132-148.

Paulay, T. (1983), "Deterministic seismic design procedures for reinforced concrete buildings", *Eng. Struct.*, **5**(1), 79-86.

Saatcioglu, M., Takayanagi, T., and Derecho, A.T. (1980), "Dynamic response of reinforced concrete wall systems", *Proc. of the 7th World Conf. on Earthquake Engineering*, **5**, 49-56.

Santhanam, T.K. (1979), "Model for mild steel in inelastic frame analysis", *J. Struct. Eng.*, ASCE, **105**(1), 199-220.

Scott, B.D., Park, R. and Priestley, M.J.N. (1982), "Stress-strain behavior of concrete confined by overlapping hoops at low and high strain rates", *ACI J.*, **79**(1), 13-17.

Stevens, N.J., Uzumeri, S.M. and Collins, M.P. (1991), "Reinforced concrete subjected to reversed cyclic shear-experiments and constitutive model", *ACI Struct. J.*, **88**(2), 135-146.

Vecchio, F.J. and Collins, M.P. (1986), "The modified compression-field theory for reinforced concrete elements subjected to shear", *ACI J.*, **83**(2), 219-231.

Volcano, A., Bertero, V.V. and Colotti, V. (1988), "Analytical modeling of R/C structural walls", *Proc. of the 9th World Conf. on Earthquake Engineering*, **VI**, 41-46.

Wu, X.H. and Lu, X.L. (1996), "A new constitutive model for nonlinear F.E. analysis of R.C. shear wall under cyclic loading", *Proc. of the 3rd Asia-Pacific Conf. on Computional Mechanics*, Korea, **2**, 1477-1482.